ELSEVIER

Coordination Chemistry Reviews
177 (1998) 97–125

COORDINATION CHEMISTRY REVIEWS

Metal–CO photodissociation in transition metal complexes: The role of ligand-field and charge-transfer excited states in the photochemical dissociation of metal–ligand bonds

E.J. Baerends [a,*], A. Rosa [b]

[a] *Afdeling Theoretische Chemie, Vrije Universiteit, 1081HV Amsterdam, Netherlands*
[b] *Dipartimento de Chimica, Universitá della Basilicata, 85100 Potenza, Italy*

Received 13 October 1997; received in revised form 4 March 1998; accepted 20 April 1998

Contents

Abstract

The photodissociation of a CO ligand from a series of d^6 metal–carbonyl complexes, with various other substituents (Cl, α-diimine, H, $Mn(CO)_5$) is discussed. The considerations are based on calculations of potential energy curves, using a density functional method. Particular attention is given to the long-standing question of the possible role of charge-transfer excited states in the photodissociation. Such CT states exist at relatively high energy (ca. 4 eV) in an unsubstituted complex like $Cr(CO)_6$, but at much lower energy if α-diimine

* Corresponding author.

PII S0010-8545(98)00128-3

ligands are introduced. For $Cr(CO)_6$, it is argued that the classical interpretation of the Cr–CO photodissociation upon excitation into the weak intensity low energy band in the spectrum at ca. 4 eV, due to the occupation of a ligand-field excited state having to be revised: the lowest excited state, from which the photodissociation occurs, has a charge-transfer character at R_e. The LF excited states are much higher in energy. They decrease in energy rapidly, however, upon Cr–CO bond lengthening, so the dissociation is due to an avoided crossing of the CT state with a LF state. This photodissociation mechanism does not depend on the nature of the lowest excited state and is shown to be operative in a variety of d^6 systems $Mn(CO)_5L$ (L = H, Cl or $Mn(CO)_5$). This immediately explains the relatively high yield of CO dissociation upon low energy excitation in $Mn_2(CO)_{10}$ and $MnCl(CO)_5$, even though the excitation is to an Mn–L σ^* LUMO orbital. Mn–L bond breaking has very different quantum yields in these compounds, which is also explained from the electronic structure. Finally, equatorial substitution with an α-diimine ligand with low-lying π^* orbitals generates $MnCl(CO)_3(\alpha\text{-diimine})$. The CT states in this case are so low that excitation does not provide enough energy for CO dissociation if the atomic configuration is kept fixed. Nevertheless, dissociation can occur by an altogether different mechanism that involves relaxation of the Cl from axial to equatorial position upon equatorial CO departure.

Keywords: Excited states; Density functional theory; Photochemistry

1. Introduction

The accepted picture of photochemical dissociation of metal–ligand bonds gives a predominant role to ligand-field excitations [1,2]. There is, however, reason to believe that the relation between the nature of the state that is populated upon irradiation and the ensuing photoreaction is less direct than has been assumed in the 'standard' model of photodissociation being induced by LF excitation. It is the purpose of this review to elucidate the mechanisms of CO dissociation in d^6 metal carbonyl complexes. We will first, in Section 3, discuss $Cr(CO)_6$ [3], which has for a long time been considered a classical case of photoreactivity in a LF excited state. The excitation spectrum of $Cr(CO)_6$ contains a low-energy low-intensity shoulder that was assigned a long time ago by Gray and Beach [4,5] to the ligand field excited state $^1T_{1g}$ belonging to the $t_{2g}^5 e_g^1$ configuration. At higher energies, the high intensity charge-transfer bands occur, with a weak band in between, which has been assigned to the $^1T_{2g}(t_{2g}^5 e_g^1)$ LF state. This assignment appeared to be confirmed by the original extended Hückel [5] as well as more recent semi-empirical INDO/S CI [6] and ab initio RHF [7] calculations. There was also little reason for revision of this assignment, since irradiation at ca. 4 eV into the low energy shoulder, presumably populating the lowest LF state, leads to photodissociation of CO. This is in perfect agreement with the expectations based on the fact that the LF transition is characterized by excitation of a t_{2g} electron to a metal–ligand antibonding e_g orbital (e.g. the d_{z^2}–5σ(CO) antibonding orbital). The Cr–CO photodissociation has been the subject of a number of time-resolved spectroscopic investigations [8–17], which have established that the dissociation is fast (within 350

fs [15]) and have mainly been directed toward the understanding of the effect of the solvent on the photodissociation dynamics and the reaction processes (vibrational relaxation and solvation). The LF nature of the photoactive excited state has not been questioned. However, we will argue (Section 3) that the interpretation of the absorption spectrum has to be revised, the low-energy low-intensity shoulder on the first high intensity CT band being in fact a symmetry forbidden CT transition rather than an LF transition [3,18]. In the calculations, the metal–CO antibonding e_g-type orbital was found to lie at relatively high energy, and the corresponding LF states lie at too high an energy to be populated by the 4 eV radiation. We will argue that photodissociation of CO nevertheless occurs since the σ-antibonding character of the e_g orbitals is not only extremely strong, it is also short-ranged. As a consequence, as soon as the metal–CO bond becomes longer, the pushing-up effect of the antibonding character rapidly diminishes, and the orbital energy and the excitation energy come down precipitously. The initially high-lying LF state is therefore characterized by a very strongly dissociative potential energy curve (PEC), which after fairly small metal–CO bond lengthening already leads to crossing with the PECs of the CT states that are lower-lying at R_e. The important implication, which is also relevant for the other complexes, is that photochemical metal–CO dissociation may take place regardless of the nature of the excited state into which the excitation takes place at equilibrium geometry.

That the situation with respect to the assumed LF nature of photoactive states may not be so simple, might, with hindsight, have been suspected from the well-known photochemistry of $Mn_2(CO)_{10}$. The HOMO and LUMO in this system are the Mn–Mn σ and σ^* orbitals. Excitation into the low-lying $\sigma \rightarrow \sigma^*$ band leads to the expected dissociation of the Mn–Mn bond, but also to a surprisingly high yield (ca. 50%) of CO dissociation. This happens in spite of a rather low percentage of CO 5σ character in these orbitals, as has been apparent for a long time from orbital composition (population analysis) data and orbital plots [19] (see also ref. [20], Fig. 13.8). The photodissociation of $Mn_2(CO)_{10}$ [21,22] is discussed in Section 5.1, but to prepare for this discussion and for the discussion of the photochemistry of other $Mn(CO)_5L$ systems, we first deal (in Section 4) with the orbital structure of the parent $Mn(CO)_5$. If in $Mn_2(CO)_{10}$, a $Mn(CO)_5$ group is replaced with Cl, to form $Mn(CO)_5Cl$, the LUMO becomes the strongly Mn–Cl antibonding σ^* orbital, yet low-energy irradiation does not lead to Mn–Cl dissociation, but leads to Mn–CO dissociation. The $MnCl(CO)_5$ [23] case is discussed in Section 5.2, and in Section 5.3 a comparison is made with $MnH(CO)_5$, where the lowest excitation is not to a σ^* orbital but is CT-like (to CO π^*, as in $Cr(CO)_6$).

One may go one step further and introduce ligands with very low-lying virtual orbitals, such as the α-diimines bpy (2,2′-bipyridine) or (with even lower lying π^* orbital) R–DAB (substituted 1,4-diaza-1,3-butadiene). Even from the very low-lying excited states that are unequivocally CT states involving an α-diimine π^* virtual orbital, CO dissociation is observed. The photoreactivity in the MLCT state of complexes containing an α-diimine ligand has been experimentally well documented, e.g. for $M(CO)_3(\alpha$-diimine) (M = Cr, Mo, W) [24–26], $M(CO)_3(\alpha$-diimine (M = Fe, Ru)[27], $Ni(CO)_2(\alpha$-diimine) [28] and the roles of LF versus CT excited

states have been carefully considered, cf. Ref. [29] and references therein. We show in Section 6 that the LF excited state is again high at the equilibrium geometry, and becomes much lower upon departure of a CO ligand. However, it does not (in the case of axial CO dissociation) or only marginally (in the case of equatorial CO dissociation) become lower than the CT state. Therefore, the CT excitation to α-diimine π^* does not provide enough energy to break the metal–CO bond. However, the system finds an altogether different, interesting mechanism by which equatorial CO dissociation (but not axial CO dissociation) can still occur.

In summary, these case studies imply that there is an important caveat against rash conclusions, on the basis of the observed photochemistry, concerning the nature of the state to which the (vertical) excitation takes place.

2. Theoretical method for calculation of the PECs

All calculations have been performed with the Amsterdam density functional (ADF) program system [30–32]. An uncontracted double-ζ STO basis set has been used with one polarization function for the C, N, O, Cl and H atoms, with one 3d and one 2p set added on Cl and H, respectively. For the metals (Cr, Mn) a triple-ζ 3d, 4s basis with one 4p function was used. The cores (C, N, O: 1s; Mn, Cr, Cl: 1s–2p) were kept frozen.

The density functionals included Becke's gradient correction [33] to the local exchange expression and Perdew's gradient correction [34] to the LDA expression (VWN [35] parametrization) for the correlation energy.

We use the ΔSCF-type method proposed by Ziegler et al. [36] for the calculation of excited states. This method has been used with good results for atomic [37–39] and molecular systems [36,40–42] as well as to the potential energy surface for the photodissociation of H_2O in its first excited state [43]. The results of the ΔSCF method are comparable with those of the theoretically better founded time-dependent DFT method [44,45] using the adiabatic local density approximation, which has recently been applied successfully to a number of simple atoms [46] and molecules [47]. A crucial element of the scheme of Ref. [36] is the restriction of total energy calculations to single-determined states only. This is a consequence of the requirements on the hole density that have to be met for the approximate functionals to be applicable. We refer to the references cited above for further details.

The DF calculations afford a straightforward interpretation of the electronic structure in terms of a molecular orbital picture. We wish to stress at this point that Kohn–Sham molecular orbitals are not just mathematical constructs whose only purpose is to build the electron density, but they are physically meaningful (see Ref. [48] and references therein), in the same way as the MOs of other one-particle models such as Hartree–Fock and extended Hückel are. This is related to the fact that the effective local potential of the Kohn–Sham model has as leading terms—apart from the nuclear potential and Coulomb potential of the total electronic density—the potential due to both the Fermi (exchange) hole and the Coulomb

hole [49–51]. The latter builds in effects of electronic correlation and in fact gives the Kohn–Sham MOs an advantage over Hartree–Fock orbitals in cases of strong near-degeneracy correlation. Virtual orbitals, being solutions in exactly the same potential as the occupied orbitals, have the advantage that they lack the artificial upshift and diffuse character of Hartree–Fock orbitals. They are useful for a qualitative interpretation of the electronic nature of excited states.

3. $Cr(CO)_6$

$Cr(CO)_6$ is a prototype d^6 system. The ligand-field splitting in the d manifold gives rise to e_g^* orbitals, that are σ-antibonding between the metal de_g orbital and a lone pair on the ligand, as illustrated for the d_{z^2} component in the well-known qualitative MO energy diagram for an octahedral d^6 transition metal complex depicted in Fig. 1. LF excitation to the e_g^* orbital reduces the number of electrons in the π-bonding t_{2g} orbitals and, more importantly, occupies the strongly antibonding Cr-d_{z^2}–CO-5σ e_g^* orbital. The excited state potential curve will be dissociative if upon Cr–CO bond lengthening the energy rise associated with the bond breaking is overcompensated by relief of the antibonding character in the excited e_g^*

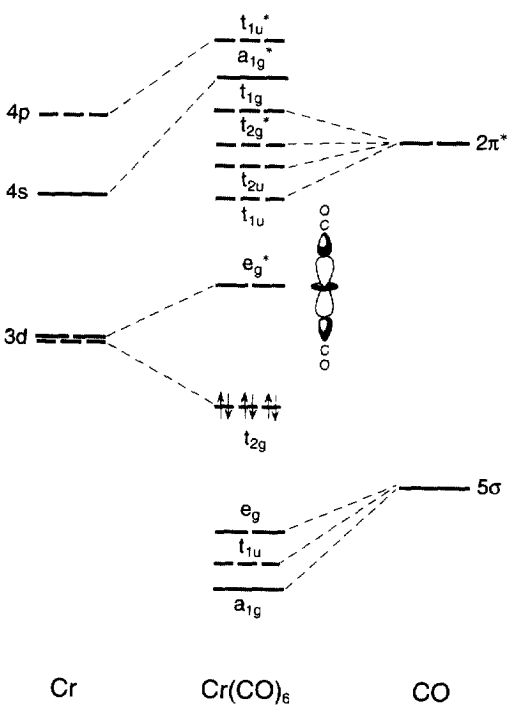

Fig. 1. Typical qualitative MO level diagram for a d^6 metal carbonyl complex, as used to picture the LF splitting and rationalize the low-energy LF excitation and photoreactivity upon low-energy absorption.

Table 1
One-electron energies and percentage composition (based on Mulliken population analysis per MO) of $Cr(CO)_6$ MOs in terms of Cr and CO fragments

MO	ε (eV)	Orbital occupancy	Cr	CO
$9a_{1g}$	0.003	0	77 (5s), 23 (4s)	
$2t_{1g}$	−0.951	0		100 ($2\pi^*$)
$6e_g$	−1.127	0	61 ($3d_{z^2}$, $3d_{x^2-y^2}$)	39 (5σ)
$3t_{2g}$	−1.574	0	39 ($3d_{xy}$, $3d_{xz}$, $3d_{yz}$)	61 ($2\pi^*$)
$2t_{2u}$	−2.165	0		100 ($2\pi^*$)
$9t_{1u}$	−2.593	0	6 ($4p_x$, $4p_y$, $4p_z$)	7 (5σ), 88 ($2\pi^*$)
$2t_{2g}$	−6.591	6	59 ($3d_{xy}$, $3d_{xz}$, $3d_{yz}$)	41 ($2\pi^*$)

orbital. In a simple one-electron picture: the rise in energy of the CO 5σ due to loss of bonding with the d_{z^2}, and of the $t_{2g}(d_\pi)$ due to loss of bonding with the leaving CO, should be overcompensated by the lowering in energy of the singly occupied e_g^*. The antibonding in the e_g^* is supposed to be so strong that this happens. The dissociation will lead to CO in the ground state and $Cr(CO)_5$ in the "t_{2g}" → "d_{z^2}" excited state. The departure of the antibonding CO will lead to strong lowering of the orbital energy of the d_{z^2}, the excitation energy in $Cr(CO)_5$ therefore being much lower than in $Cr(CO)_6$. If one makes the balance, it is clear that the energy available for the breaking of the Cr–CO bond is just the difference in excitation energy in the initial complex and in the photoproduct.

This traditional picture of the photodissociation in $Cr(CO)_6$ (and in general) as occurring from the LF excited state is not correct, although it certainly contains elements of truth. In Table 1, the Kohn–Sham orbital energies of the 3d orbitals, the highest occupied orbital $2t_{2g}$ and the empty $6e_g$ orbital, are given, as well as those of the whole set of empty CO $2\pi^*$ orbitals and the Cr 4s orbital. We note that the $6e_g$ orbital is not the LUMO, as is assumed in the traditional MO scheme of Fig. 1, but is actually quite high up in the virtual orbital spectrum. The spread in the CO $2\pi^*$ orbitals is substantial, amounting to more than 1.5 eV. It is caused by bonding and antibonding interactions between the CO molecules of the $(CO)_6$ cage. As a matter of fact, the spread is larger in the empty $(CO)_6$ cage since the lowest one in the cage is the mostly strongly CO–CO bonding t_{2g} combination of $2\pi^*$ orbitals, which in the complex is shifted up considerably by the π-antibonding with the $3d\text{–}t_{2g}$ orbitals. The σ-antibonding present in the $6e_g$ is, however, so strong that it puts the $6e_g$ orbital (nominally 3d) even higher, close to the top of the $2\pi^*$ band (in a Hartree–Fock calculation we found the same picture, with actually the $6e_g$ even above the whole $2\pi^*$ band). We note that the mixing between the 3d orbitals and the CO orbitals is strong in both the π bond (the $2t_{2g}/3t_{2g}$ bonding/antibonding set) and the σ bond ($5e_g/6e_g$). The $6e_g$ is nominally a 3d orbital and the $3t_{2g}$ is nominally a $2\pi^*$ orbital, but both have ca. 40% admixture of other orbitals.

The orbital energies suggest that the LF states will not be the lowest states in the excitation spectrum. We do indeed find that the lowest excited states are the a^1T_{2u}, a^1E_u and a^1A_{2u} that arise from $2t_{2g} \rightarrow 9t_{1u}$ CT ($3d \rightarrow 2\pi^*$) excitation (we will restrict

ourselves to the singlet states). The excitation energies are calculated to be 4.0–4.2 eV. The same $(2t_{2g})^5(9t_{1u})^1$ configuration also leads to the much higher lying a^1T_{1u} state. These results agree with CASSCF/CASPT2 [18] calculations with respect to the ordering of the excited states. These calculations, which may be considered the most sophisticated ones to date, find, in agreement with our DF calculations, and contrary to the previous calculations [6,7], the LF excited states to be at much higher energy than has been assumed before. The DFT excitation energies are higher (typically some 0.5 eV) than the CASPT2 ones, the CASSCF energies being again some 1–1.5 eV higher (the PT2 corrections are large). We do obtain, however, the same ordering of the excited states: both the DFT and CASSCF/CASPT2 calculations find first the above-mentioned a^1T_{2u}, a^1E_u, a^1A_{2u} set, followed by the b^1E_u, a^1A_{1u}, b^1T_{2u} set of states arising from the next CT transition, the $2t_{2g} \rightarrow 2t_{2u}$ orbital excitation. Again the fourth state belonging to this excited configuration, b^1T_{1u}, is at much higher energy. The excitations from the ground state to a^1T_{1u} and b^1T_{1u} are the only ones allowed by both spin and spatial symmetry, cf. the discussions by Beach and Gray [5] and Pierloot et al. [18]. The crucial point for our discussion is that the lowest excitations are calculated to be the a^1T_{2u}, a^1E_u, a^1A_{2u} and b^1E_u, a^1A_{1u}, b^1T_{2u} sets of symmetry forbidden charge transfer excitations, not LF excitations. The lowest LF state originating from the $(2t_{2g})^5(6e_g)^1$ configuration is found in both the DFT (5.2 eV) and the CASSCF/CASPT2 (4.85 eV) calculations at substantially higher energy, in fact in the same energy range as the symmetry allowed CT excitations to a^1T_{1u} and b^1T_{1u}.

The calculations thus strongly indicate that the LF excited states are too high to be directly populated upon irradiation at ca. 4.0 eV. The low intensity of the absorption at this energy is to be attributed to their symmetry forbidden nature, not to their LF character.

In order to investigate the observed photochemical metal–CO dissociation upon irradiation at this energy, we have calculated the PECs along the Cr–CO dissociation coordinate for the states arising from the $2t_{2g} \rightarrow 9t_{1u}$ CT excitation. The curves as shown in Fig. 2 have been obtained while keeping the geometry of the $Cr(CO)_5$ fragment constant along the dissociation coordinate. The PECs demonstrate that there are, in spite of the CT character of the states derived from the $2t_{2g} \rightarrow 9t_{1u}$ excitation, two dissociative or nearly dissociative PECs, of $^1B_2$ and ^1E symmetry in the relevant C_{4v} point group, arising from the a^1T_{2u} and a^1E_u states. The corresponding triplet states (not shown) are both purely dissociative. This demonstrates that it is not necessary to excite to LF states in order to induce photodissociation of ligands, but that the dissociation may also occur from CT states. The observed photoactivity may therefore not be used for assigning the low-energy absorption to LF excitation. It should also be noted that the singlet PECs are dissociative, so that it is not necessary to invoke intersystem crossing to the dissociative triplet PECs in order to explain the photodissociation. In agreement with this, Joly and Nelson [17] concluded from their transient absorption measurements that the photodissociation proceeds directly from the initially excited state with no intersystem crossing necessary.

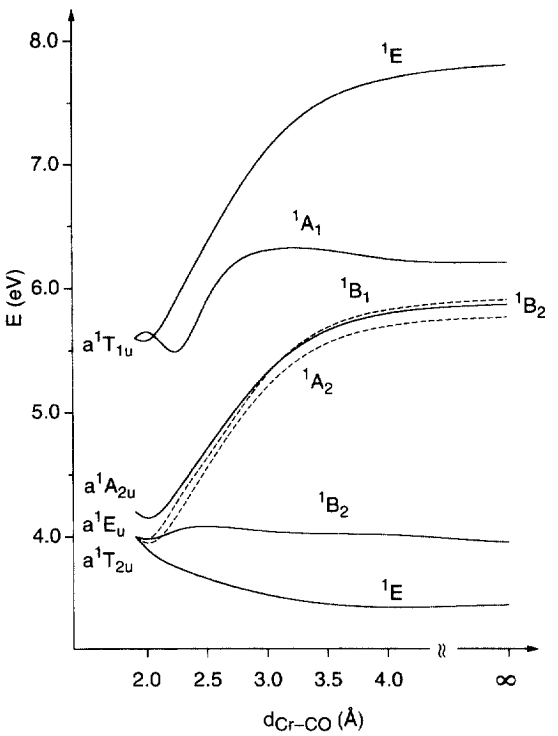

Fig. 2. PECs along the Cr–CO dissociation coordinate for the singlet states (in C_{4v} symmetry) arising from the lowest excited (charge-transfer) configuration, $(2t_{2g})^5(9t_{1u})^1$.

It is possible to understand from the electronic structure why this excitation is photoactive, and one can indeed predict immediately that precisely these B_2 and E PECs will be the dissociative ones. The essential element in the explanation is that, even though the excitation is to a CT state at R_e, the dissociation is still driven by the presence of a strongly dissociative LF state that is at high energy at R_e but rapidly lowers its energy upon CO bond lengthening. The symmetry of the dissociative LF state, which can be predicted without calculation, then dictates B_2 and E symmetry for the dissociative PECs in Fig. 2, as will be detailed below.

Upon Cr–CO bond lengthening, the antibonding present in the Cr-d_{z^2}–CO-5σ e_g^* orbital (we will denote it as "d_{z^2}") rapidly diminishes. It will come down and cross with lower lying virtual levels, or exhibit an avoided crossing in case of equal symmetry, and will ultimately become the lowest virtual orbital. This implies that the LF state corresponding to the excitation to "d_{z^2}" starts at high energy but is strongly dissociative and will become the lowest excited state eventually. We should caution that, due to the presence of a remaining *trans* CO ligand, with high ligand field strength, the case of $Cr(CO)_6$ is actually slightly more complicated than this picture suggests, for the d_{z^2} character not only ends up in the low-lying $Cr(CO)_5$ LUMO, but also appears in a higher lying a_1 orbital. Since this is an important

point for the photochemistry of the $Mn(CO)_5L$ systems—($Mn(CO)_5$ has very much the same orbital structure as $Cr(CO)_5$)—we discuss this point in somewhat more detail. Let us consider the splitting of the relevant orbitals upon lowering the symmetry from O_h to C_{4v}:

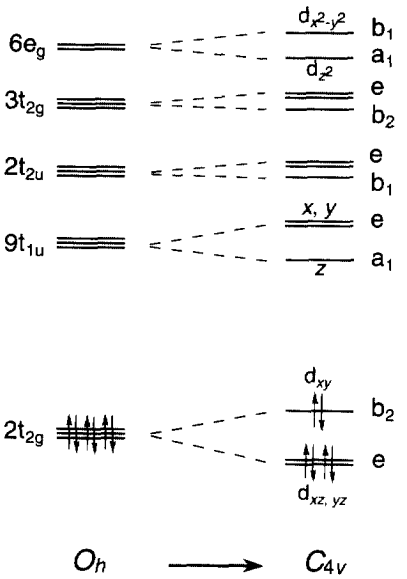

The Cr-d_{z^2}–CO-5σ e_g^* orbital has an a_1 symmetry in C_{4v}, just as one of the components of the $9t_{1u}$ orbitals. When an axial CO is moved away, this "d_{z^2}" orbital will come down. We would expect this $a_1(6e_g)$ orbital to exhibit an avoided crossing with the $a_1(9t_{1u})$. This means that the states arising from the $2t_{2g} \rightarrow a_1(9t_{1u})$ CT excitation, under the symmetry lowering have become either $e(2t_{2g}) \rightarrow a_1(9t_{1u})$ or $b_2(2t_{2g}) \rightarrow a_1(9t_{1u})$, i.e. having E or B_2 symmetry in C_{4v} will have an avoided crossing with E or B_2 LF states arising from the $e(2t_{2g}) \rightarrow a_1(e_g)$ and $b_2(2t_{2g}) \rightarrow a_1(e_g)$ excitations, respectively. These LF states are strongly dissociative. The avoided crossing may result in a barrier on the PEC, but if the crossing is strongly avoided no barrier will appear. It is actually found completely lacking in ^1E and to be weak in $^1B_2$ (see Fig. 2). Indeed, in the calculations, the orbital energies of the $a_1(6e_g)$ and the $a_1(9t_{1u})$ orbitals never come very close; the $a_1(6e_g)$ does come down in energy initially, but it does not get close to the lower lying $a_1(t_{1u})$ since at larger Cr–CO bond distances (2.0 Å and beyond), the $a_1(9t_{1u})$ energy actually drops faster. So we do not have the simple picture that the $a_1(6e_g)$, characterized by a significant d_{z^2} character, on its way down crosses the $a_1(9t_{1u})$, characterized by zero d_{z^2} character, at R_e as well as at larger distances. The character of these orbitals changes in a somewhat more complicated way. Along the Cr–CO dissociation coordinate, these two orbitals gradually but considerably mix, with the symmetry lowering also

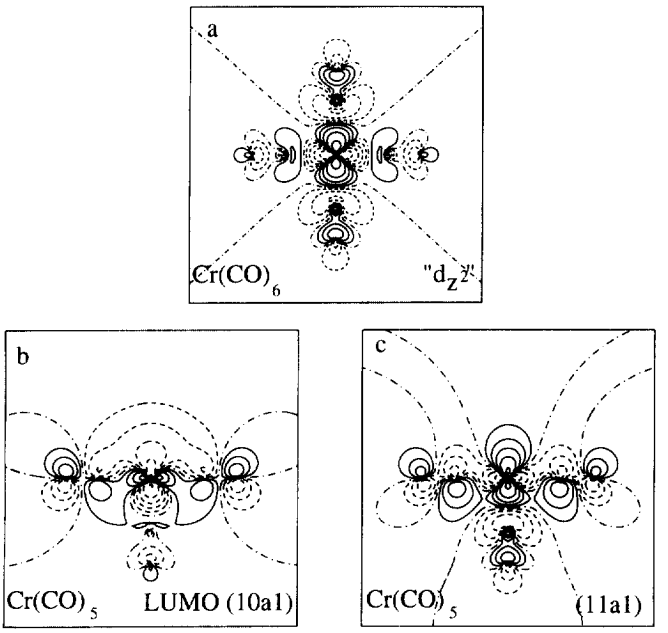

Fig. 3. (a) Orbital contour plot of the virtual e_g^* ("d_{z^2}") orbital of $Cr(CO)_6$. Contour values: ± 0.5, ± 0.2, ± 0.1, ± 0.05, ± 0.02 and 0.0 (e bohr^{-1})$^{1/2}$. (b) Orbital contour plot of the a_1 LUMO of $Cr(CO)_5$, which is similar to the $10a_1$ SOMO of $Mn(CO)_5$. (c) Orbital contour plot of the $11a_1$ σ' orbital of $Cr(CO)_5$ (similar to $11a_1$ of $Mn(CO)_5$).

giving rise to other orbital admixing, such as $4p_z$. Ultimately the LUMO of $Cr(CO)_5$, which evolves smoothly from the $a_1(9t_{1u})$, has about as much d_{z^2} character as the higher lying a_1 orbital, the latter however incorporating all of the antibonding with the axial CO that is left behind. Since the a_1 LUMO of $Cr(CO)_5$, which is essentially similar to the singly occupied a_1 SOMO of the $Mn(CO)_5$ fragment, plays, together with the next higher a_1 orbital, an important role in the understanding of the photochemistry of the $Mn(CO)_5L$ systems, we will discuss these orbitals in some detail in the Section 4. The change in going from $a_1(6e_g)$ (i.e. "d_{z^2}") to the a_1 LUMO of $Cr(CO)_5$ can be appreciated by comparing the contour plots of these orbitals in Fig. 3(a) and (b). The plot of the $Cr(CO)_5$ LUMO shows the strong mixing of equatorial CO $2\pi^*$ with Cr $4p_z$ and $3d_{z^2}$ in this orbital. In view of the hybrid nature of the a_1 LUMO of $Cr(CO)_5$ one cannot unequivocally denote excitation to this orbital either as LF or as CT excitation. Nevertheless, this a_1 LUMO has much lower energy than the original $a_1(e_g)$ orbital; it is in fact much lower than the lowest $2\pi^*$ orbital, so that it is situated in the energy window between the highest occupied 3d levels and the start of the CO $2\pi^*$ manifold. The low position of this LUMO corresponds to a low first excitation energy in $Cr(CO)_5$. The first excitation energy in $Cr(CO)_5$ is so much lower than the first excitation energy in $Cr(CO)_6$ that the difference is enough to provide the energy to dissociate CO.

So the picture that the Cr–CO dissociation from a state that has CT character at R_e can be understood from the (strongly avoided) crossing of this state by a strongly dissociative LF state captures the essence of the electronic structure explanation of the photochemical CO dissociation in the case of $Cr(CO)_6$.

It is clear now that amongst the states that arise from the $2t_{2g} \rightarrow 9t_{1u}$ excitation those that can be derived from orbital excitation to the a_1 component (in C_{4v} symmetry) of the $9t_{1u}$ will be the ones that can give rise to states with dissociative PECs, either with a barrier or barrierless. The $e(2t_{2g}) \rightarrow a_1(9t_{1u})$ and $b_2(2t_{2g}) \rightarrow a_1(9t_{1u})$ excitations give rise to E and B_2 states in C_{4v}, respectively. All the other states from the $(2t_{2g})^5(9t_{1u})^1$ configuration in O_h, corresponding to $e \rightarrow e$ excitation (A_1, A_2, B_1 and B_2 states in C_{4v}) and $b_2 \rightarrow e$ excitation (E state in C_{4v}) are not expected to be dissociative. This is corroborated by the calculations of the PECs (see Fig. 2). Most of the PECs ($^1A_2$, $^1B_2$, $^1B_1$, ^1E) simply curve upward, the energy rising due to the loss of bonding to the leaving CO. The behaviour of the $^1A_1$ state arising from the a^1T_{1u} is somewhat different and is discussed in Ref. [3].

We conclude that the photodissociation of CO does not occur because of the LF character of the first excited state, but because of the crossing of the lowest excited state by the rapidly descending, initially high lying, LF excited state. In the case of $Cr(CO)_6$, the lowest excited state at R_e was of CT-type. However, the mechanism of CO photodissociation that we have identified here does not depend on the nature of the lowest excited state. It will, therefore, be very interesting to investigate cases where the lowest excited state is changed by the introduction of substituents. In Section 5 we will discuss $Mn(CO)_5L$ systems, where L is a one-electron ligand, which may lead to a lowest excitation to an Mn–L σ^* LUMO, as in the case of $L = Mn(CO)_5$, in $Mn_2(CO)_{10}$ and L = Cl in $MnCl(CO)_5$. Substitution of equatorial COs by an α-diimine ligand introduces very low lying π^* orbitals in the virtual orbital spectrum. CO photodissociation from the corresponding very low lying CT states is the subject of Section 6. However, before dealing with the photochemistry, we investigate in Section 4 the electronic structure of the $Mn(CO)_5$ fragment, since the perturbation on the octahedral environment resulting from the vacant coordination site plays a crucial role in the understanding of the electronic structure of the $Mn(CO)_5L$ systems and their photochemistry.

4. The a_1 hybrid SOMO of $Mn(CO)_5$

Before we discuss the photochemistry of $Mn(CO)_5L$ systems, it is useful to consider the structure of the most important orbitals of $Mn(CO)_5$. One might in a simplified picture assume that the perturbation of the local octahedral environment in a hexacarbonyl by removing one CO ligand at the z-axis, would result in the splitting of the degenerate $3d-e_g$ set, the d_{z^2} orbital becoming lower in energy due to loss of antibonding with the leaving CO [52]. We have noticed above that indeed a hybrid with considerable d_{z^2} character becomes the low lying LUMO in $Cr(CO)_5$. However, Fig. 3(b) demonstrates that there is considerable admixing of $2\pi_{eq}$ and metal $4p_z$, so that a hybrid is created with high amplitude at the vacant site and

good acceptor properties. A second remarkable feature of this LUMO (which is the $10a_1$ orbital counting valence levels only) is the lack of antibonding with the remaining axial CO 5σ. As detailed in Ref. [21], there is a second, higher lying $11a_1$ orbital (see Fig. 3(c)), located in the middle of the $2\pi^*$ band, that has as much d_{z^2} character as the $10a_1$ LUMO and that does have a significant contribution of the axial CO (16.9% against 2.5% in $10a_1$), which is strongly antibonding (the Mn–CO_{ax} overlap population is -0.202 in the $11a_1$ and $+0.004$ in the $10a_1$). This second orbital is crucial for the understanding of the photochemistry of the $Mn(CO)_5L$ compounds. As is apparent from Fig. 3(c), there are other differences between $10a_1$ and $11a_1$: for instance, $10a_1$ has considerable $4p_z$ character; $11a_1$ has virtually none. Both have considerable (ca. 50%) $2\pi_{eq}$ character (the largest contribution percentage-wise), but with opposite phases (with respect to d_{z^2}).

It is possible to understand the composition of these orbitals using Scheme 1. The first point that should be realized is the importance of the strong interaction between the $4p_z$ and the a_1 combination of 2π orbitals on the equatorial COs (the ones with their lobes perpendicular to the equatorial plane). The $4p_z$ overlaps strongly with the $a_1(2\pi_{eq})$ ($S = 0.66$). We will have to account for this large overlap and strong interaction in a qualitative interaction diagram like Scheme 1. In this scheme, we start with $3d_{z^2}$ and $4p_z$ orbitals that each have been destabilized by

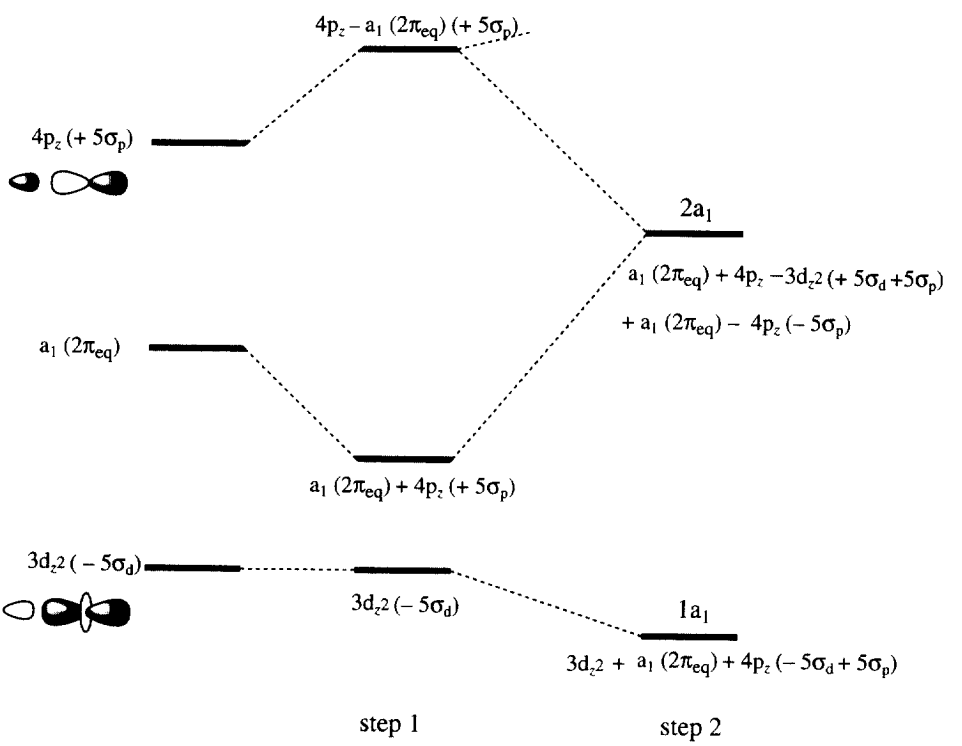

Scheme 1.

antibonding with the CO_{ax} 5σ. The contribution of $5\sigma_{ax}$ to the $3d_{z^2}$ to form the $3d_{z^2}(-5\sigma_d)$ combination, is larger than the mixing of $5\sigma_{ax}$ with $4p_z$ to form the (antibonding) $4p_z(+5\sigma_p)$ combination (we denote small admixtures between parentheses; the d and p subscripts distinguish the admixing of $5\sigma_{ax}$ to the 3d and 4p, respectively). The $a_1(2\pi_{eq})$ is strongly stabilized by the in-phase interactions between the $2\pi_{eq}$ orbitals on the adjacent equatorial carbonyls and is in between the destabilized $4p_z(+5\sigma_p)$ and $3d_{z^2}(-5\sigma_d)$. In the first step we allow the only strong interaction to take place, i.e. the $a_1(2\pi_{eq})$ with $4p_z$ mixing. This will bring the bonding combination $a_1(2\pi_{eq})+4p_z(+5\sigma_p)$, which is essentially the $a_1(2\pi_{eq})$ pushed down by the $4p_z$, close to the $3d_{z^2}(-5\sigma_d)$. From the final orbital composition we deduce that these two levels must be so close that considerable mixing occurs in the second step. The stabilized orbital that results from this mixing in step 2 is the hybrid orbital $10a_1 = a_1(2\pi_{eq}) + 3d_{z^2} + 4p_z(-5\sigma_d + 5\sigma_p)$ (the AOs are listed in order of importance, the small contribution in parentheses). The large $a_1(2\pi_{eq})$ and $4p_z$ contributions to this orbital are evident from the contour plot of Fig. 3(b). The partial cancellation of the $5\sigma_d$ and $5\sigma_p$ contributions explains the small amount of 5σ character in the $10a_1$. The $11a_1$ arises from two effects, the first being the antibonding mixing of $3d_{z^2}(-5\sigma_d)$ with the $a_1(2\pi_{eq})+4p_z(+5\sigma_p)$. This mixing is determined by the $a_1(2\pi_{eq})+4p_z$ with $5\sigma_d$ and the $3d_{z^2}$ with $5\sigma_p$ interactions. In the second place there is bonding admixture ('pushing down') by the $4p_z$-$a_1(2\pi_{eq})(+5\sigma_p)$. The $4p_z$ contributions cancel each other but the $2\pi_{eq}$ contributions reinforce each other, resulting in the large $2\pi_{eq}$ character found in the $11a_1$. Note that the relative phases of $3d_{z^2}$ and $a_1(2\pi_{eq})$ in the $10a_1$ and $11a_1$ orbitals are opposite. Note also that considerable $5\sigma_{ax}$ character remains in $11a_1$, its antibonding with $3d_{z^2}$ not being diminished by bonding with $4p_z$, hence giving the large negative $Mn-CO_{ax}$ overlap population mentioned before. The reversal of phase of the $a_1(2\pi_{eq})$ implies that in the $11a_1$ orbital the $5\sigma_{ax}$ will also be antibonding with the equatorial COs. We may therefore expect that antibonding with axial CO will strongly increase upon population of this orbital in an electronic excitation. On the other hand, the absence of antibonding with axial CO in the $10a_1$ is noticeable.

5. Photochemistry of $Mn(CO)_5L$ systems, $L = Mn(CO)_5$, Cl, R

The $Mn(CO)_5$ radical, with one electron in the $10a_1$ SOMO, may bind to various one-electron ligands. The photochemistry of such compounds may be rather different, depending on the nature of the L ligand. In the case of $L = Mn(CO)_5$, we obtain $Mn_2(CO)_{10}$, which has the σ-bonding orbital between the two $10a_1$ orbitals as HOMO, and the corresponding σ^* as LUMO. The $\sigma \rightarrow \sigma^*$ excitation leads to Mn–Mn bond breaking, and simultaneously to CO dissociation, with approximately equal quantum yields. At higher excitation energies the CO dissociation becomes increasingly more predominant. As a matter of fact, CO dissociation is always, with any ligand L, an important photoreaction. The breaking of the σ bond is, however, very much dependent on the nature of L. If L = Cl no Mn–Cl bond homolysis occurs; if L = H very little Mn–H homolysis occurs; but, if $L = CH_3$ or

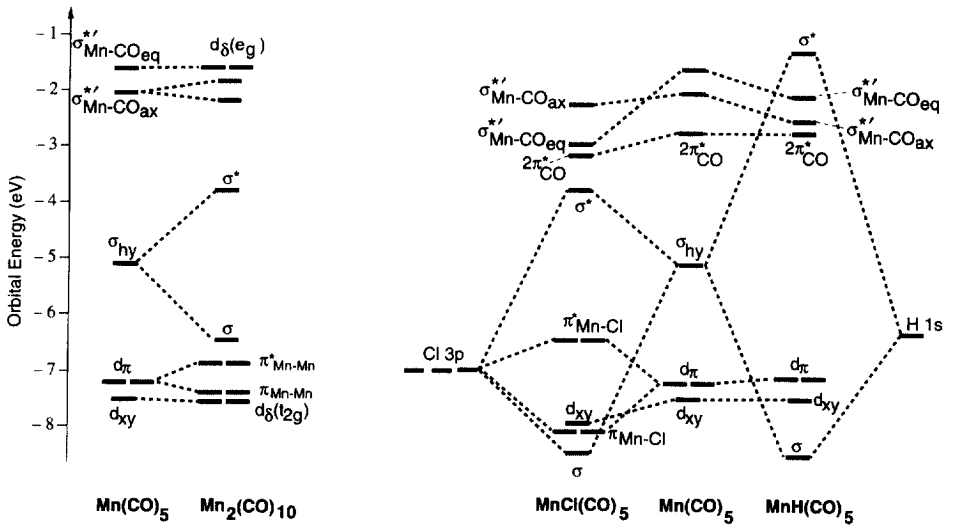

Fig. 4. Orbital interaction diagram for the formation of $Mn(CO)_5L$, where $L = Mn(CO)_5$, Cl or H. The Cl 3p level is not at the energy calculated in the neutral atom but is positioned so as to suggest correctly the composition of the orbitals.

$CH_2C_6H_5$, Mn–R bond breaking occurs more readily. We will discuss the photochemistry of the $Mn(CO)_5L$ compounds, with $L = Mn(CO)_5$, $L = Cl$ and $L = R$ separately, using the orbital energy diagrams of Fig. 4 to help us distinguish the differences and similarities.

5.1. $Mn_2(CO)_{10}$

For $Mn_2(CO)_{10}$, the dissociation coordinates that have been considered [22] are indicated in Scheme 2. In the calculated PECs D_{4d}, C_{4v} and C_s symmetries were retained along the reaction paths corresponding to the homolysis of the Mn–Mn bond, the loss of an axial and an equatorial CO, respectively. Along the Mn–Mn and the $Mn-CO_{ax}$ coordinates all geometrical parameters except for the dissociating bond were optimized.

Considering first the breaking of the Mn–Mn bond we note that the relevant frontier orbital of the $Mn(CO)_5$ fragment, indicated here as the σ_{hy} orbital, is the $10a_1$ $a_1(2\pi_{eq})$-$4p_z$-d_{z^2} hybrid orbital (singly occupied) discussed in Section 4. If we bring two $Mn(CO)_5$ fragments together to form $Mn_2(CO)_{10}$, the σ_{hy} orbitals form bonding and antibonding combinations (the occupied σ HOMO and empty σ^* LUMO, respectively). The HOMO is very close to occupied 3d orbitals ('t_{2g}'-type orbitals in the local octahedral environment), the highest one of which is the Mn–Mn π antibonding $d_\pi^* = d_\pi(Mn_1) + d_\pi(Mn_2)$ orbital. The lowest excited states, that will be involved in a typical photochemical experiment, are the $d_\pi^* \rightarrow \sigma*$ ($^{1,3}E_1$) and the $\sigma \rightarrow \sigma^*$ ($^{1,3}B_2$) states. From the allowed $^1B_2(\sigma \rightarrow \sigma*)$ state the system may reach through intersystem crossing the $^3B_2$, which has been calculated [22] to be

purely dissociative, as expected for the triplet state corresponding to bonding → antibonding orbital excitation in a simple electron pair bond. This straightforwardly explains the Mn–Mn bond homolysis. The situation with respect to Mn–CO dissociation is rather more involved. We have stressed the lack of antibonding with the CO_{ax} 5σ lone pair orbital in the σ_{hy} of $Mn(CO)_5$ (and therefore in the σ and σ^* orbitals of $Mn_2(CO)_{10}$). One would therefore expect the PECs along the $Mn-CO_{ax}$ dissociation coordinate of the lowest excited states not to be dissociative. However, there is amongst the virtual orbitals the much higher lying, strongly $Mn-CO_{ax}$ σ-antibonding, $11a_1$ orbital in $Mn(CO)_5$. This orbital is in fact more entitled to the denomination de_g-type orbital, since it incorporates the $3d_{z^2}$-$5\sigma_{ax}$ antibonding. We use a prime to distinguish this orbital from the σ_{hy}: σ', or, if we wish to stress the σ antibonding character with the axial CO ligand, $\sigma^{*\prime}$ (see Fig. 4). We now find a very similar behaviour of this 'e_g' orbital as is observed in the case of $Cr(CO)_6$: when the axial CO is removed, the loss of antibonding causes this orbital to come down in energy precipitously. It crosses all lower virtual levels and becomes the LUMO already around $R(Mn-CO_{ax}) = 2.2$ Å. So the LF excited states corresponding to $\sigma \rightarrow \sigma'$ or $d_\pi^* \rightarrow \sigma'$ excitation, are at high energy at R_e but drop in energy very quickly and cross the lowest excited states with $\sigma \rightarrow \sigma^*$ or $d_\pi^* \rightarrow \sigma*$ character. The

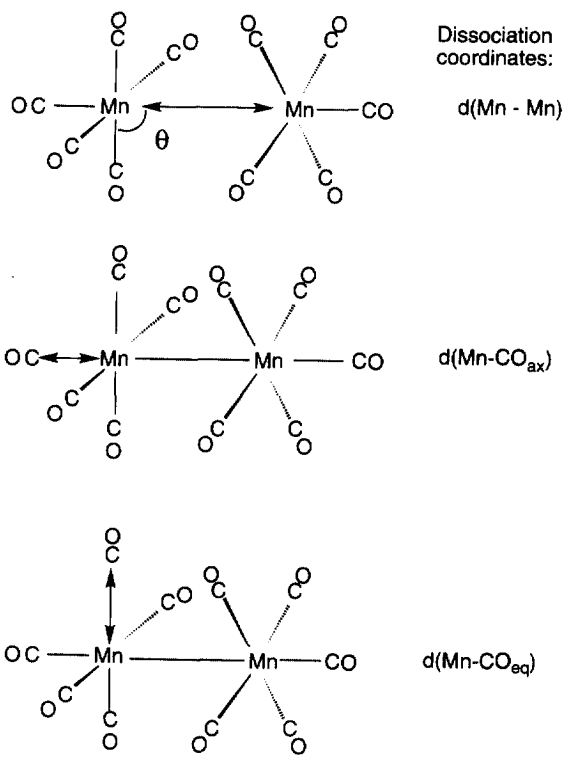

Scheme 2.

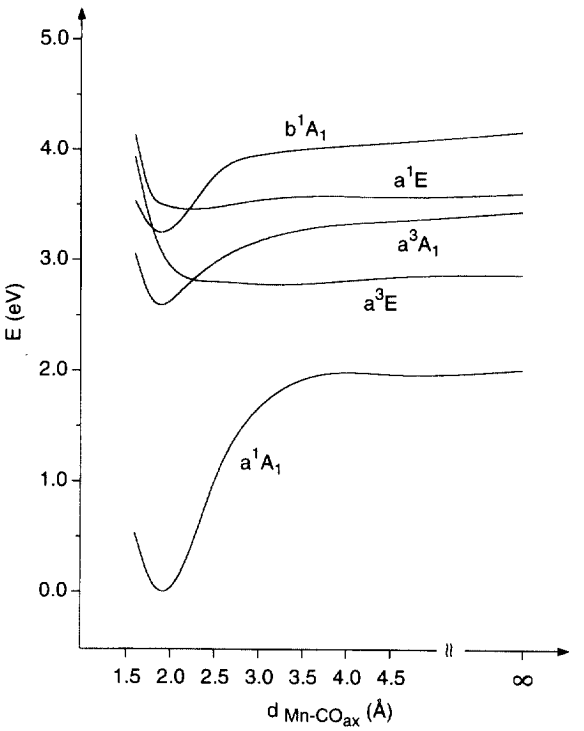

Fig. 5. PECs for the dissociation of the $Mn-CO_{ax}$ bond in $Mn_2(CO)_{10}$.

latter have $^{1,3}A_1$ and $^{1,3}E$ symmetry, respectively, in C_{4v}. Our calculations showed (see Fig. 5) that the $^{1,3}A_1$ PECs have a bonding minimum around R_e. This bonding minimum is, however, much less deep than the one in the $^1A_1$ ground state curve, since the down-coming $A_1(\sigma \rightarrow \sigma')$ crosses the excited state $^{1,3}A_1$ PECs rather soon. The crossing is actually avoided, it shows up in a gradual change of the electronic character of the excitation from $\sigma \rightarrow \sigma^*$ to $\sigma \rightarrow \sigma'$ character along the excited state $^{1,3}A_1$ PECs. There is not a barrier in the PECs, owing to the fact that the $A_1(\sigma \rightarrow \sigma')$ state comes down so fast and the crossing is strongly avoided. Turning now to the $^{1,3}E$ PECs corresponding to excitation out of d_π^*, we note (see Fig. 5) that these do not even show a bonding minimum but are almost completely dissociative. This difference with the $^{1,3}A_1$ PECs can be understood as follows. The excitation $d_\pi^* \rightarrow \sigma*$ transfers one of the four $d_\pi - 2\pi_{ax}^*$ bonding electrons to an orbital with virtually no CO_{ax}–metal bonding or antibonding character. One would therefore expect some bond lengthening in this excited state, but no bond breaking. The bond lengthening means that the E PECs are expected to curve upwards at a somewhat longer $Mn-CO_{ax}$ distance than the A_1 PECs. At the same time, however, the $E(d_\pi^* \rightarrow \sigma')$ excited state comes down more rapidly, and more deeply. This is due to the fact that, in addition to the σ' coming down upon $Mn-CO_{ax}$ bond lengthening, the d_π^* orbital goes up in energy, being destabilized by the loss of π bonding with the $2\pi*$

orbital of the leaving CO. As pictured in Fig. 4 of Ref. [22], the d_π^* ($8e_3$ in D_{4d}, 16e in C_{4v}) is below the $10a_1$-σ_{hy} at R_e but crosses it and becomes the HOMO at ca. 2.2 Å. The $E(d_\pi^* \rightarrow \sigma')$ excited state therefore drops particularly rapidly, and it crosses the $E(d_\pi^* \rightarrow \sigma*)$ so soon that the PEC of this latter state has no room to curve upward. Asymptotically, in $Mn_2(CO)_9$, the $E(d_\pi^* \rightarrow \sigma')$ excitations (singlet and triplet) are at lower energies than the singlet and triplet $A_1(\sigma \rightarrow \sigma')$ excitations, respectively. The net effect is that the PECs of the first singlet and triplet E excited states are purely dissociative, whereas those of the first A_1 excited states still exhibit a bonding minimum, although not very deep.

We will discuss the photochemical dissociation of the equatorial COs only briefly, and refer to Ref. [22] for details. The situation for equatorial CO dissociation in the $Mn(CO)_5L$ systems is simpler than for axial CO dissociation, and more analogous to the situation in $Cr(CO)_6$, since the $d_{x^2-y^2}$ component of the d-e_g set of orbitals is not perturbed by the loss of one of the ligands that interacts with it. It does not exhibit the phenomenon of 'division' over a low-lying 'σ' and a higher lying 'σ'', as is the case for the d_{z^2}-e_g upon loss of the axial CO; see the discussion in Section 4. The $d_{x^2-y^2}$-e_g orbital is located in the virtual orbital spectrum of $Mn(CO)_5$ above the high lying $\sigma'(d_{z^2})$, since it is still 'pushed up' by four equatorial 5σ lone pair orbitals, and is also denoted as σ' (see Fig. 4). When an $Mn-CO_{eq}$ bond distance is lengthened, this orbital comes down in energy and rehybridizes so as to get more amplitude at the empty coordination site. This hybrid orbital becomes the lowest virtual orbital asymptotically (in $Mn_2(CO)_9$ with an empty equatorial coordination site), although it remains somewhat higher in energy than the hybrid resulting upon axial CO loss, owing to the three equatorial COs that still exert an antibonding 'pushing up' effect. The excited state of $Mn_2(CO)_9$ that results asymptotically, which will have the hybrid orbital occupied, will be at somewhat higher energy than in the case of axial CO loss, although of course the initially high lying $\sigma \rightarrow \sigma'(d_{x^2-y^2})$ and $d_\pi^* \rightarrow \sigma'(d_{x^2-y^2})$ excited states also come down (the $d_\pi^* \rightarrow \sigma'$ the most) very strongly in this case. They will cross the $\sigma \rightarrow \sigma^*$ and $d_\pi^* \rightarrow \sigma*$ excited states, which are the lowest ones at R_e. The behaviour of the PECs of the lowest excited states corresponding to $Mn-CO_{eq}$ dissociation (these PECs have been obtained while keeping all geometrical parameters fixed except for the $Mn-CO_{eq}$ distance) thus becomes analogous to the PECs corresponding to axial CO dissociation; some minor differences arise from the fact that the $\sigma'(d_{x^2-y^2})$ comes down somewhat less and somewhat more slowly upon Mn–CO bond lengthening. Owing to the symmetry lowering to C_s the $E(d_\pi^* \rightarrow \sigma*)$ state now splits into A′ and A″ states. Again the states that start as $\sigma \rightarrow \sigma^*$ excitations at R_e are not dissociative with respect to the $Mn-CO_{eq}$ bond, exhibiting a fairly shallow bonding minimum close to R_e, but the $^3A'$ component of the $^3E(d_\pi^* \rightarrow \sigma*)$ excited state is dissociative. Its PEC is different from the corresponding ^3E for axial CO dissociation: it is very flat and has to pass a low barrier [22].

Summarizing, we find that the low-energy excitation that will populate the $\sigma \rightarrow \sigma^*$ excited state and will lead to Mn–Mn bond breaking, may also lead to CO dissociation by the same mechanism as observed for $Cr(CO)_6$: rapid lowering of the high-lying LF excited states, so that they will cross the lowest excited states (in

particular $d_\pi^* \rightarrow \sigma*$) and make the corresponding PEC dissociative. As a matter of fact, since the electronic nature of the lowest excited state at equilibrium geometry is not decisive for the mechanism of photochemical metal–CO dissociation that we are proposing, it is not so surprising, with hindsight, that Mn–CO dissociation occurs from the lowest excited state of $Mn_2(CO)_{10}$ with $\sigma \rightarrow \sigma^*$ character, just as Cr–CO photodissociation occurs from the lowest excited state of $Cr(CO)_6$ with MLCT character. The lowest excited state at R_e need not be an LF excited state, although of course its energy with respect to the asymptotic energy of the resulting LF excited state (low-lying!) in $Mn_2(CO)_9$ is important.

5.2. $Mn(CO)_5Cl$

When we consider next the $Mn(CO)_5Cl$ system, we immediately observe in Fig. 4 a few relevant differences with $Mn_2(CO)_{10}$. In the first place, the σ bonding orbital between Cl and the $Mn(CO)_5$ fragment is at much lower energy, occurring below the occupied d-t_{2g} orbitals. The occupied p_π orbitals of Cl make bonding and antibonding combinations with the d_π orbitals of the d-t_{2g} set, so that a relatively high lying Mn–Cl π antibonding HOMO results. The LUMO is a σ antibonding orbital between the σ_{hy} of the $Mn(CO)_5$ fragment and the Cl p_σ orbital. As in the case of $Mn_2(CO)_{10}$, we have amongst the virtual orbitals two with σ antibonding character with axial ligands: the first one is the σ^* LUMO which is Mn–Cl antibonding, the second one is the analogue of the $11a_1$-σ' orbital of the $Mn(CO)_5$ fragment which is $Mn–CO_{ax}$ σ antibonding (to emphasize this antibonding character it is also denoted $\sigma^{*\prime}$). This orbital is practically unperturbed by the bonding with Cl. Calculation of the excitation energies [23] shows that the lowest excited state corresponds to the excitation out of the π^*(Mn–Cl) HOMO to the σ^*(Mn–Cl) LUMO. In this case, however, there is, in contrast to $Mn_2(CO)_{10}$, no Mn–L σ bond breaking observed. The primary photoprocess is CO dissociation (see Scheme 3 for the relevant dissociation coordinates; the geometry of the TM fragment has been kept frozen for the PEC calculations along the dissociation coordinates).

The fact that no Mn–Cl bond homolysis occurs may be explained from the PECs displayed in Fig. 6. The Mn–Cl bond (calculated at 297 kJ mol^{-1} for unrelaxed $Mn(CO)_5$ fragment, and at 268 kJ mol^{-1} after relaxation) is much stronger than the Mn–Mn bond (calculated in the range 112–114 kJ mol^{-1} [53]). The E($\pi^* \rightarrow \sigma^*$) states that are populated when the irradiation takes place in the first absorption band are calculated to lie below the asymptotic energy of the free $Mn(CO)_5$ and Cl radicals. Excitation to these states therefore does not supply enough energy to homolytically break the Mn–Cl bond and the absence of Mn–Cl homolysis is attributed to the high thermodynamic stability of the Mn–Cl bond.

If Mn–Cl dissociation were to occur, it would be expected to be along a dissociative (at least in the asymptotic limit) $^3A_1(\sigma \rightarrow \sigma*)$ PEC. There is indeed a $^3A_1$ state correlating with the $^2A_1 + {}^2P$ ground state of the radicals, which corresponds from ca. 2.7 Å onwards to the Mn–Cl $\sigma \rightarrow$ Mn–Cl σ^* $21a_1 \rightarrow 22a_1$ transition. The a^3A_1 PEC has the expected dissociative behaviour in the asymptotic tail. However, at the equilibrium geometry the lowest $^3A_1$ state is not the $^3A_1(\sigma \rightarrow \sigma*)$,

but it is the a^3A_1 state arising from the $13e(\pi^*(Mn-Cl)) \rightarrow 14e(CO\text{-}2\pi^*)$ transition. This excited state has at R_e much lower energy than the $^3A_1(\sigma \rightarrow \sigma*)$ state but it is not dissociative, so an avoided crossing with the strongly dissociative $^3A_1(\sigma \rightarrow \sigma*)$ state will occur. The barrier resulting from the avoided crossing is clearly visible on the calculated a^3A_1 PEC in Fig. 6. The $\sigma \rightarrow \sigma^*$ excitation energy has been calculated at shorter distances than 2.7 Å, and a sketch of the steeply descending $\sigma \rightarrow \sigma^*$ state is given in Fig. 6 without, however, trying to map out in detail the avoided crossings through which the $\sigma \rightarrow \sigma^*$ character descends (except for the last one). Excitation to the b^1A_1, a^3A_1 ($13e \rightarrow 14e$) at R_e or to nearby higher excited states can only yield the radical products after crossing the barrier in the a^3A_1 PEC. In this region many states are present (not drawn in Fig. 6) and internal conversion towards lower states will probably be rather fast. As a consequence, Mn–Cl bond homolysis is unlikely. It is in fact not even observed with high energy radiation [54], although a low quantum yield for Mn–Cl bond breaking would theoretically certainly be possible.

The different position of the Mn–Cl σ bonding orbital, and the resulting different (much higher) $\sigma \rightarrow \sigma^*$ excitation energy in $MnCl(CO)_5$ compared with $Mn_2(CO)_{10}$, in addition to the higher Mn–L bond strength, thus explains the difference in Mn–L photochemical σ bond breaking probabilities. With respect to Mn–CO bond breaking, however, there is not much difference. Again the Mn–CO

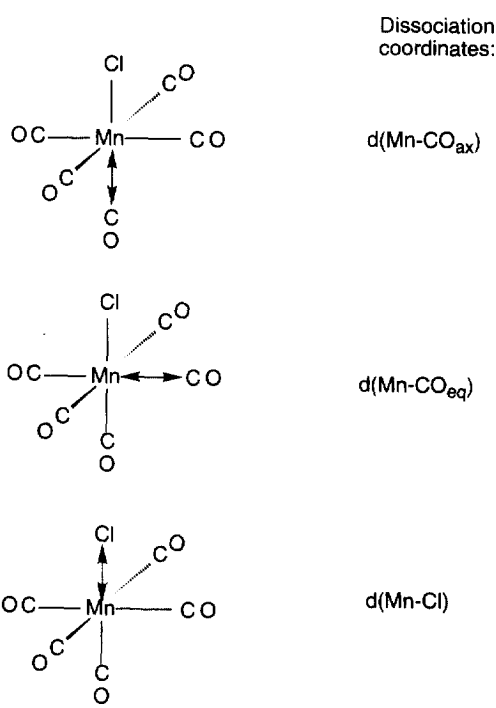

Scheme 3.

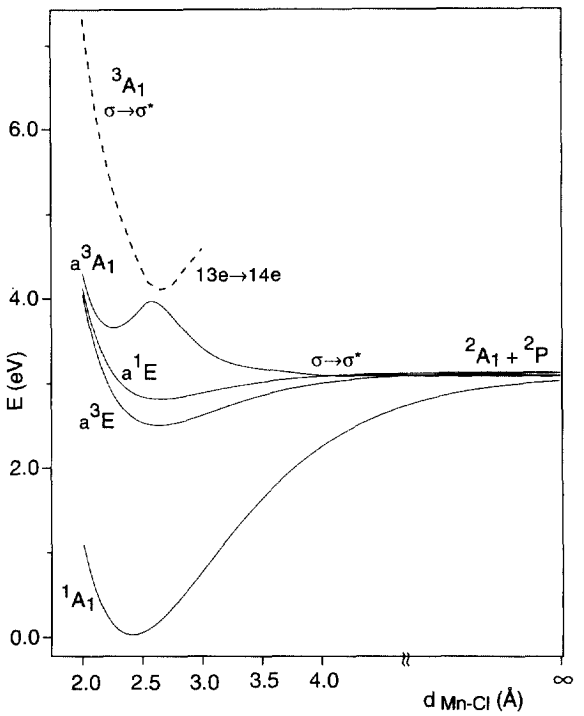

Fig. 6. PECs for Mn–Cl bond homolysis. The avoided crossing between the two $^3A_1$ states is not calculated accurately and is only indicated.

antibonding orbitals, denoted as σ', which are high-lying at R_e, come down upon Mn–CO bond lengthening, and the corresponding LF excited states come down too and cross the lowest excited state of p, $d_\pi^* \rightarrow \sigma*$ character (the 13e HOMO is the d_π–p_π antibonding orbital, which we denote p, d_π^*). The PECs of the lowest excited states along the Mn–CO_{ax} dissociation coordinate are dissociative. They have $^{1,3}E(d_\pi \rightarrow \sigma*)$ character at R_e, and change to $^{1,3}E(p, d_\pi^* \rightarrow$ "d_{z^2}" $- \sigma')$ character asymptotically. Along the Mn–CO_{eq} dissociation coordinate the $^{1,3}A'$ components of the $^{1,3}E$ in the lower (C_s) symmetry are dissociative. They exhibit a similar change of electronic character, to $d_{xz} \rightarrow$ "$d_{x^2-y^2}$"-σ' character asymptotically (the leaving CO is along the x-axis). We find [23] that for both axial and equatorial CO dissociation the triplet PECs are purely dissociative, the singlet PECs exhibiting a very slight barrier. So when irradiation of $MnCl(CO)_5$ with low energy light has resulted in occupation of the a^{1}E state, the excited molecules can either lose axial (*trans*-) or equatorial (*cis*-) CO after overcoming only a small barrier in both directions, or undergo intersystem crossing to the a^{3}E state. From this latter state axial and equatorial CO loss can occur without any barrier. Indeed, photochemical *cis*- and *trans*-CO exchange has been observed in ^{13}CO exchange experiments [55]. It should, however, be cautioned that this does not strictly prove the occurrence of both primary photoprocesses, since fast rearrangements may also occur during

these exchange processes. Our results do point to the occurrence of both reactions. In this respect they do not substantiate the assumption that photochemical *trans*-CO dissociation is most likely for this type of complex. This assumption has been generally made, based on the expectation that the CO dissociation was occurring out of the lowest LF excited state, the nature of which was assumed to be "d_{z^2}" since the opposite Cl has weaker ligand field strength than CO. These assumptions created a problem in view of the experimental result that, upon irradiation of metal pentacarbonyl halides in the presence of a Lewis base, trans-substituted photoproducts are totally absent. The exclusive dissociation of axial CO has not been questioned, but an explanation for the lack of trans-substituted photoproducts has been sought [54] in rapid rearrangement of the apical $MnCl(CO)_4$ primary photoproduct to $MnCl(CO)_4$ with Cl in the basal plane. This point has recently been studied in detail by Pierloot et al. [56] and Matsubara et al. [57]. Since we find the mechanism for CO dissociation not to be related to the nature of the lowest excited state, which we would not classify as LF but rather as p, $d_\pi^* \rightarrow \sigma*$, we find both equatorial and axial CO loss to be possible. Since we certainly cannot exclude *trans*-CO loss, the results of the studies on the rapid excited state rearrangement of the apical $MnCl(CO)_4$ system are relevant for the present work as well.

As for the PECs of higher excited states [23], we have found the A″ components of the next higher E states (b^3E and b^1E), to be also dissociative for equatorial CO loss, but not for axial CO. The presence of these states can account for the increase in quantum yield when going to shorter wavelength excitation. It is then expected that the ratio of equatorial to axial CO loss changes in favour of equatorial CO loss when the wavelength of excitation is shortened.

5.3. $Mn(CO)_5R$

Further variation of the ligand L in $Mn(CO)_5L$ to for instance L = H or alkyl (methyl, ethyl, benzyl) or phenyl is possible. The photochemistry may be rather different for the Mn–L bond breaking, but the Mn–CO photodissociation is rather similar in all cases, which is consistent with the photodissociation mechanism proposed here. It needs no further comment. The different behaviour with respect to the homolysis for different ligands R, for instance much more readily CH_3 dissociation than H dissociation, may be rationalized in terms of the character of the lowest excited states, which in turn is related to the molecular orbital energy diagram. The case of $MnH(CO)_5$ has been studied by Daniel [58] using CASSCF/CCI calculations. In Fig. 4, we show the orbital energies for $MnH(CO)_5$. The important difference with L = Cl is the very high position of the Mn–H σ^* orbital in the virtual spectrum. It is actually above the σ' orbitals that are $Mn–CO_{ax}$ and $Mn–CO_{eq}$ antibonding. This implies that the $\sigma \rightarrow \sigma^*$ excited state, whose triplet component will be strongly dissociative, is at too high energy at R_e to be populated directly in the usual photochemical experiment. The $^3(\sigma \rightarrow \sigma*)$ (of $^3A_1$ symmetry) will at longer distances become much lower in energy, and asymptotically it will connect to the ground states of the radical fragments. We therefore expect that this dissociative curve will—possibly after other avoided crossings—eventually cross

the lowest $^3A_1$ state, making the lowest $^3A_1$ PEC dissociative at long distances. However, the lowest $^3A_1$ state at equilibrium geometry, corresponding to the $d_\pi \rightarrow 2\pi^*(CO)$ excitation, is at much lower energy than $^3A_1(\sigma \rightarrow \sigma*)$, and there will develop a considerable barrier in the lowest $^3A_1$ PEC, before the avoided crossing to the dissociative outer part occurs. This has actually been observed in the calculations of Daniel [58]. The poor quantum yield for Mn–H bond dissociation is thus easily explained.

6. MLCT photochemistry of α-diimine-substituted d^6 metal complexes

An interesting variation in the orbital structure and excitation spectrum occurs upon introduction of an α-diimine ligand, as in $MnL(CO)_3$(α-diimine) systems. The α-diimine ligands such as 2,2′-bipyridine, 1,10-phenanthroline or 1,4-diaza-1,3-butadiene (DAB) are characterized by two donating N lone pairs that will occupy adjacent ligand sites, and a low-lying (lower than CO $2\pi^*$) π^* orbital. Very low lying metal $\rightarrow \pi^*$ MLCT excited states therefore result. Although MLCT states are usually unreactive and have long lifetimes, the photoreactivity of the low lying MLCT states of α-diimine complexes is now well documented. Several mechanisms—dissociation from directly populated MLCT states, from long-lived ^{3}MLCT states, or from LF states thermally populated via MLCT states—have been proposed, but are still controversial. PECs have been calculated by Finger and Daniel [59] for both Mn–H dissociation and $Mn-CO_{ax}$ dissociation, and the Mn–H dissociation has been studied using quantum mechanics (wave packet evolution) for the nuclear dynamics [60]. Finger and Daniel obtained one strongly dissociative $^3A''$ PEC and two nearly dissociative $^3A'$ PECs for $Mn-CO_{ax}$ dissociation. Much more work remains to be done to unravel fully the mechanisms and relative quantum yields of the various reaction channels for the MLCT states.

We wish briefly to discuss here the remarkable photochemistry of the *fac*-$MnCl(CO)_3$(α-diimine) complexes [61], with an axial Cl instead of H ligand, since this provides an example where a photochemical CO dissociation pathway occurs [62], i.e. altogether different from those discussed above. Irradiation of the *fac*-$MnCl(CO)_3$(bpy) complex does not lead to loss of the halide, but it does give rise to release of a carbonyl ligand. Remarkably, back-reaction with CO, thermally and photochemically, gives exclusively *mer*-$MnCl(CO)_3$(bpy) isomer with Cl in an equatorial position

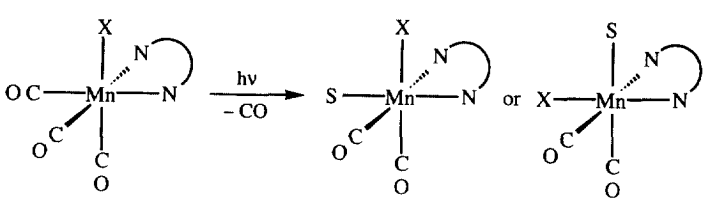

Scheme 4.

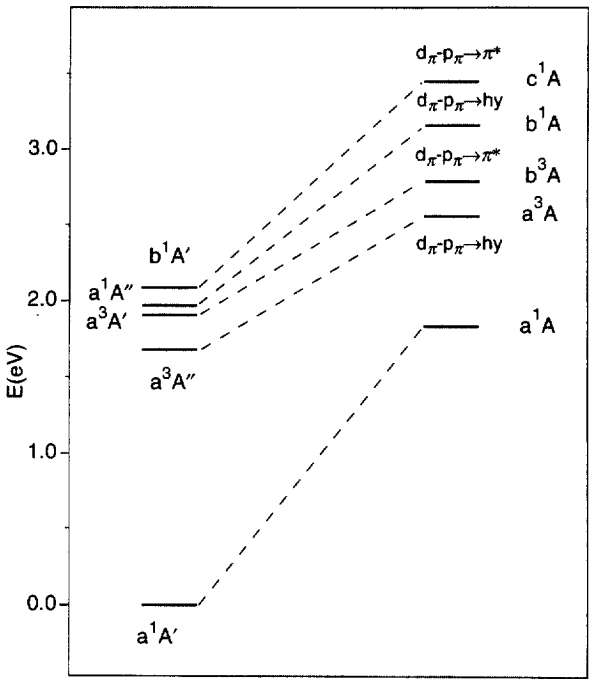

Fig. 7. Correlation diagram for ground and lowest excited states of the 'reactant' (*fac*-$MnCl(CO)_3$(H–DAB) at equilibrium geometry) and the CO loss 'product' in the frozen **1b** geometry.

trans to one of the N atoms of the α-diimine. (The *mer* isomer thermally transforms back to the *fac* isomer, or photodecomposes into radicals Cl and $Mn(CO)_3(bpy)^{\cdot}$, but we will not be concerned with these further reactions.) It has been experimentally established that the primary product following CO loss is a solvento species with a *cis,cis* conformation, i.e. the two carbonyls are *cis* to each other and the halide and solvent ligands are *cis* to each other as well. This leaves us with the two possible structures depicted in Scheme 4, so the question remains as to whether the halide occupies an axial or an equatorial position in the primary photoproduct.

These two structures do seem to rule out the dissociation of an axial CO *trans* to the Cl as primary photoreaction. We have verified that indeed *trans*-CO dissociation is not likely, the lowest excited states exhibiting a bonding minimum in the $Mn-CO_{ax}$ coordinate. Equatorial CO dissociation leads, if we freeze the geometry of the $MnCl(CO)_2$(H–DAB) fragment, to very similar electronic structure effects as have been observed in the other cases: the "$d_{x^2-y^2}$" σ' antibonding orbital comes down in energy rapidly and hybridizes so as to create as LUMO a hybrid (denoted 'hy') with high amplitude at the vacated equatorial site. There is also a very low lying π^* virtual orbital on the α-diimine ligand. The hy orbital still becomes asymptotically lower, but not very much so. This illustrates the problem with low lying CT states: if the hy orbital does not come very much lower than the α-diimine π^* orbital, the

excitation energy to the hy orbital in the photoproduct will not be much smaller than the CT excitation energy to the π^* in the initial complex (or, for that matter, in the photoproduct). But it is this difference that has to provide the energy for the breaking of the bond. Fig. 7 demonstrates that indeed the low lying CT excited states at R_e are below the lowest excited states in the product five-coordinated complex, which are of d, p → hy type (with the CT d, p → π^* excitations next). If the lowest excited states at R_e were not the low-energy MLCT states introduced by the α-diimine, but were 1 eV higher, say, the asymptotically very low lying d, p → hy excited state would offer the possibility of a dissociative lowest excited state PEC by the by now familiar crossing to the d, p → hy state with a low or no barrier. However, with the α-diimine present the MLCT state is already at low energy to begin with; the d, p → hy state does not cross with it at moderately elongated $Mn-CO_{eq}$ distances, but only asymptotically becomes somewhat lower in energy than the d, p → π^* state. The lowest excited state PEC, therefore, will not be dissociative in the case of (approximate) retention of the atomic configuration. This incidentally offers an illustration of why photoreactivity may be very low in MLCT states.

How, then, can we explain the observed CO dissociation in the MLCT excited state in this particular complex? The answer appears from calculations where at each point along the $Mn-CO_{eq}$ dissociation coordinate the geometry of the rest of the system is optimized, as schematically indicated in Scheme 5.

It has been found [62] that equatorial CO dissociation actually does not proceed with approximate retention of the atomic configuration, as assumed in the discussion above. This is already apparent when an automatic geometry optimization is performed on the CO_{eq} loss product, starting with the frozen geometry of the initial complex. In such a geometry optimization the Cl ligand does not retain its apical position, but it bends down to the vacated equatorial site. The energy is lowered by 60 kJ mol^{-1} during this relaxation of the metal fragment. Effectively an axial vacancy results, which will be occupied by a solvent molecule or by CO upon back reaction with CO. This ties in very well with the observation that only the *mer*-$MnCl(CO)_3(bpy)$ complex results in the photosubstitution reaction. Here one would have to assume that the release of an equatorial CO ligand is not so fast, compared with the relaxation motion of Cl towards the equatorial plane, that a

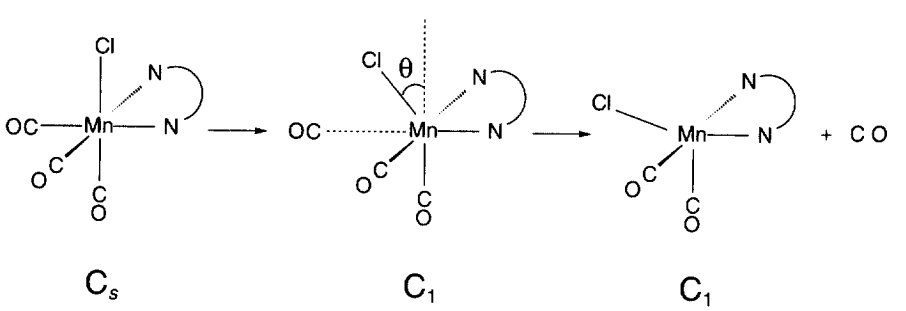

Scheme 5.

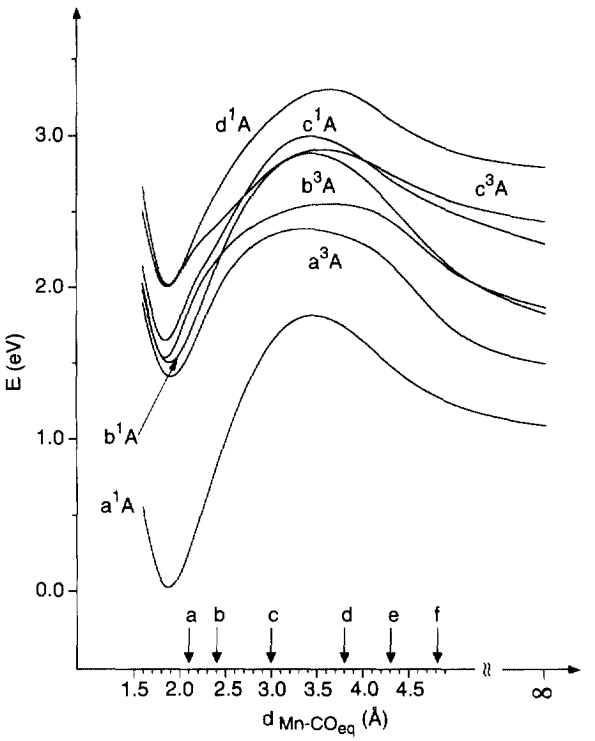

Fig. 8. PECs for the dissociation of the Mn–CO_{eq} bond in *fac*-$MnCl(CO)_3$(H–DAB). The arrows indicate Mn–CO_{eq} distances at which the Cl bending has occurred to the following $\angle(CO_{eq}–Mn–Cl)$ angles: (a) 82.0°; (b) 82.6°; (c) 76.4°; (d) 65.6°; (e) 61.8°; (f) 49.5°; ∞, 16.7°.

substituting ligand (solvent molecule) could occupy the equatorial site before it is occupied by Cl. It is interesting to investigate what precisely occurs during the CO_{eq} dissociation, and we have therefore calculated the ground state PEC along the Mn–CO_{eq} dissociation coordinate, optimizing at each Mn–CO_{eq} distance all geometric parameters. Excitation energies at each point have been calculated using the optimized (at a given Mn–CO_{eq} bond distance) ground state geometry, although separate geometry optimizations in selected excited states at various Mn–CO_{eq} distances have been performed to check if substantial rearrangements occur in the excited states (which proved not to be the case). Fig. 8 shows that the ground state PEC as well as the excited state PECs have a remarkable maximum at rather large Mn–CO_{eq} distance (larger than 3 Å in all cases). This is the distance at which the Cl starts to bend down to the equatorial plane in order to occupy the coordination site that CO is leaving. Much of the Mn–CO bond breaking has occurred at that point, although CO has not left completely, and the PEC goes down again as a result of the energy gained by the shift in position of Cl. There results a considerable barrier in the ground state PEC. A similar barrier is found in the excited state PECs, which all represent MLCT excited states, from the occupied metal 3d-t_{2g} orbitals to the α-diimine π^*.

It is clear from Fig. 8 that the equatorial carbonyl ligand will hardly be able to dissociate along the excited state PECs because of the high potential barrier (no less than 95 kJ mol^{-1}). The clear minimum around the equilibrium distance in the excited state PECs agrees with the electronic nature of these MLCT states, in which no Mn–CO antibonding orbital is occupied. Although CO_{eq} loss cannot, therefore, occur directly along the lowest excited state PECs of *fac*-$MnCl(CO)_3$(H–DAB), our calculations suggest that $Mn–CO_{eq}$ bond breaking may occur through an alternative mechanism where the topology of the ground state PEC plays a key role. According to the shape of the ground state PEC, continuum states in the $Mn–CO_{eq}$ coordinate will exist at all energies above the asymptotic energy. According to the well-known resonance phenomenon of continuum states above a potential well, the continuum states describing the nuclear motion of leaving CO will at certain energies have an enhanced amplitude ('resonance') in the potential well region (around R_e) reminiscent of the vibrational states in the discrete part of the spectrum. Radiationless transition from the MLCT states to such a continuum state belonging to the ground state PEC may lead to dissociation, either directly if the transition takes place to a continuum state above the maximum of the barrier or by thermal excitation (rather than tunnelling) if the transition is to a state just below the maximum. This process would of course occur on a much longer time scale than the rapid ejection (20–200 fs) [15,63,64] along strongly dissociative excited state PECs. This long time scale is consistent with the use of the fully relaxed ground state PEC, since time is available for the presumably slow motion of the Cl to the equatorial position.

The crucial factor in this reaction mechanism is the energy lowering following the movement of the halide from the *fac*- to *mer*-position. If the rearrangement is concurrent with the CO_{eq} dissociation, the experimentally observed *fac*- to *mer*-isomerization is automatically explained: after the first reaction step, free CO, still present in solution, may easily react with the five-coordinated intermediate, $MnCl(CO)_2$(H–DAB), to give the *mer*-$MnCl(CO)_3$(H–DAB) isomer.

Summarizing, we have proposed a mechanism for $Mn–CO_{eq}$ dissociation in *fac*-$MnCl(CO)_3$(H–DAB) in which the topology of the ground state energy surface plays a key role. The mechanism is certainly different from that proposed for metal–ligand bond breaking in the $Cr(CO)_6$ and $Mn(CO)_5L$ complexes. In the latter complexes, the non-reactive lowest excited state, of CT character ($Cr(CO)_6$) or of $\sigma \rightarrow \sigma^*$ or $d \rightarrow \sigma^*$ character ($Mn(CO)_5L$), is crossed by a reactive LF state. In the *fac*-$MnCl(CO)_3$(H–DAB) the lowest MLCT states appear to have too low an energy for this mechanism to work. However, an alternative dissociation route, involving strong relaxation of the photoproduct, seems to be possible.

7. Summary

We conclude that the role of LF excited states in the photochemistry of TM complexes may be somewhat different than has been generally assumed. We find that LF excitations are at relatively high energy at R_e. In the case of $Cr(CO)_6$ the

low-energy shoulder in the spectrum has been attributed [5] to an LF excited state, which appeared to be in agreement with the low intensity as well as its leading to photolytic metal–CO bond cleavage. We find in agreement with Pierloot et al. [18] that symmetry-forbidden transitions to low energy CT states should be responsible for the absorption in the low energy regime (ca. 4.0 eV). Some of these CT states are calculated to be dissociative, accounting for the experimentally observed photoactivity. The mechanism that makes the states dissociative is in essence (see above for details) the rapid lowering upon Cr–CO bond lengthening of Cr–CO antibonding LF states that are high-lying at R_e. The antibonding in the e_g^* orbital, to which the excitation takes place in the LF excited states, is strong, causing the high excitation energy, but it also appears to be rather short-ranged, causing the orbital energy to drop rapidly upon bond lengthening. The lowering of the LF excited state causes it to cross the lowest excited state, which is in $Cr(CO)_6$ of MLCT nature ($3d\text{-}t_{2g} \rightarrow CO\text{-}2\pi^*$). We have found the same mechanism to apply in a number of $Mn(CO)_5L$ systems: CO dissociation occurs due to high-lying LF states descending rapidly upon Mn–CO bond lengthening, and crossing with non-dissociative lower states. Since this appears to be a general mechanism, the CO dissociation occurs generally, with little or no relation to the nature of the lowest excited state at R_e. It is not necessary to excite to LF states in order to induce photodissociation of ligands, and such dissociation, when observed, does not prove that the excitation was to an LF state. However, the accepted picture that metal–ligand dissociation occurs from LF excited states, is based on an underlying assumption, namely, that LF states are dissociative, which is fully corroborated by the calculations: they actually are so strongly dissociative that even if they are too high to be populated directly by irradiation into the lowest absorption band, they cross so soon with the lowest excited states that the lowest excited state PEC becomes dissociative.

These results fit in nicely with the experimental observations that a primary photoprocess of all these complexes is Mn–CO dissociation, with higher quantum yield for higher energy radiation due to increased $Mn\text{–}CO_{eq}$ dissociation. In $Mn_2(CO)_{10}$ the Mn–Mn bond homolysis is fully competitive with Mn–CO bond dissociation upon irradiation in the lowest band (1:1), with the propensity to Mn–CO bond breaking increasing at higher energy. In $MnH(CO)_5$ and $MnCl(CO)_5$ Mn–H/Cl bond homolysis occurs much less readily. Mn–H bond dissociation only occurs upon irradiation with high energy, but in much lower yield than Mn–CO bond dissociation, whereas for $MnCl(CO)_5$ no Mn–Cl bond homolysis has (yet) been found. The difference between these systems with respect to the Mn–Mn/H/Cl homolysis can be understood immediately from the positions of the σ and σ^* molecular orbitals (Fig. 4).

Acknowledgements

The authors wish to thank Giampaolo Ricciardi, Maikel Wilms and Christoph Pollak for their contributions to the work described here. Professor D.J. Stufkens

of the University of Amsterdam has stimulated the authors' interest in the photochemistry of metal–ligand bonds and has provided many suggestions and challenges. A grant of computer time from the Stichting Nationale Computerfaciliteiten (NCF) of the Netherlands Organization for Scientific Research (NWO) is gratefully acknowledged.

References

[1] G.L. Geoffroy, M.S. Wrighton, Organometallic Photochemistry, Academic Press, New York, 1979.
[2] G.J. Ferraudi, Elements of Inorganic Photochemistry, Wiley, New York, 1988.
[3] C. Pollak, A. Rosa, E.J. Baerends, J. Am. Chem. Soc. 119 (1997) 7324.
[4] H.B. Gray, N. Beach, J. Am. Chem. Soc. 85 (1963) 2922.
[5] N.A. Beach, H.B. Gray, J. Am. Chem. Soc. 90 (1968) 5731.
[6] M. Kotzian, N. Rösch, H. Schröder, M.C. Zerner, J. Am. Chem. Soc. 111 (1989) 7687.
[7] K. Pierloot, J. Verhulst, P. Verbeke, L.G. Vanquickenborne, Inorg. Chem. 28 (1989) 3059.
[8] J.K. Burdett, J.M. Grzybowski, R.N. Perutz, M. Poliakoff, J.J. Turner, R.F. Turner, Inorg. Chem. 17 (1978) 147.
[9] D.P. Gerrity, L.J. Rothberg, V. Vaida, J. Phys. Chem. 87 (1983) 2222.
[10] J.M. Kelly, C. Long, R. Bonneau, J. Phys. Chem. 87 (1983) 3344.
[11] T.R. Fletcher, R.N. Rosenfeld, J. Am. Chem. Soc. 107 (1985) 2203.
[12] J.D. Simon, X. Xie, J. Phys. Chem. 90 (1986) 6751.
[13] R.A. Seder, S.P. Church, E.J. Weitz, J. Am. Chem. Soc. 108 (1986) 4721.
[14] L. Wang, X. Zhu, K.G. Spears, J. Am. Chem. Soc. 110 (1988) 8695.
[15] A.G. Joly, K.A. Nelson, J. Phys. Chem. 93 (1989) 2876.
[16] M. Lee, C.B. Harris, J. Am. Chem. Soc. 111 (1989) 8963.
[17] A.G. Joly, K.A. Nelson, Chem. Phys. 152 (1991) 69.
[18] K. Pierloot, E. Tsokos, L.G. Vanquickenborne, J. Phys. Chem. 100 (1996) 16545.
[19] W. Heijser, E.J. Baerends, P. Ros, Discuss. Faraday Soc. (Symp.) 14 (1980) 211.
[20] J.K. Burdett, Molecular Shapes. Theoretical Models of Inorganic Stereochemistry, Wiley, New York, 1980.
[21] A. Rosa, G. Ricciardi, E.J. Baerends, D.J. Stufkens, Inorg. Chem. 34 (1995) 3425.
[22] A. Rosa, G. Ricciardi, E.J. Baerends, D.J. Stufkens, Inorg. Chem. 35 (1996) 2886.
[23] M.P. Wilms, E.J. Baerends, A. Rosa, D.J. Stufkens, Inorg. Chem. 36 (1997) 1541.
[24] H.K. van Dijk, P.C. Servaas, D.J. Stufkens, A. Oskam, Inorg. Chim. Acta 104 (1985) 179.
[25] S. Wieland, K. Bal Reddy, R. van Eldik, Organometallics 9 (1990) 1802.
[26] J. Víchová, F. Hartl, A. Vlcek Jr., J. Am. Chem. Soc. 114 (1992) 10903.
[27] H.K. van Dijk, D.J. Stufkens, A. Oskam, J. Am. Chem. Soc. 111 (1989) 541.
[28] P.C. Servaas, D.J. Stufkens, D.J. Oskam, Inorg. Chem. 28 (1989) 1780.
[29] A. Vlcek Jr., J. Víchová, F. Hartl, Coord. Chem. Rev. 132 (1994) 167.
[30] E.J. Baerends, D.E. Ellis, P. Ros, Chem. Phys. 2 (1973) 41.
[31] G. te Velde, E.J. Baerends, J. Comput. Phys. 99 (1992) 84.
[32] C. Fonseca Guerra, O. Visser, J.G. Snijders, G. te Velde, E.J. Baerends, in: E. Clementi, G. Corongiu (Eds.), Methods and Techniques for Computational Chemistry, STEF, Cagliari, 1995, p. 305.
[33] A. Becke, Phys. Rev. A 38 (1988) 3098.
[34] J.P. Perdew, Phys. Rev. B 33 (1986) 8822 (Erratum: Phys. Rev. B 34 (1986) 7406).
[35] S.H. Vosko, L. Wilk, M. Nusair, Can. J. Phys. 58 (1980) 1200.
[36] T. Ziegler, A. Rauk, E.J. Baerends, Theor. Chim. Acta 43 (1977) 261.
[37] U. von Barth, Phys. Rev. A 20 (1979) 1693.
[38] J.H. Wood, J. Phys. B 13 (1980) 1.
[39] M. Lannoo, G.A. Baraff, M. Schlüter, Phys. Rev. B 24 (1981) 943.

[40] T. Ziegler, A. Rauk, Theor. Chim. Acta 46 (1977) 1.
[41] A. Rosa, E.J. Baerends, Inorg. Chem. 33 (1994) 584.
[42] C. Daul, E.J. Baerends, P. Vernooijs, Inorg. Chem. 33 (1994) 3538.
[43] M.-L. Doublet, G.J. Kroes, E.J. Baerends, A. Rosa, J. Chem. Phys. 103 (1995) 2538.
[44] E. Runge, E.K.U. Gross, Phys. Rev. Lett. 52 (1984) 997.
[45] E.K.U. Gross, W. Kohn, Adv. Quantum Chem. 21 (1990) 255.
[46] M. Petersilka, U.J. Gossmann, E.K.U. Gross, Phys. Rev. Lett. 76 (1996) 1212.
[47] C. Jamorski, M. Casida, D.R. Salahub, J. Chem. Phys. 104 (1996) 5134.
[48] E.J. Baerends, O.V. Gritsenko, R. van Leeuwen, in: B.B. Laird, R.B. Ross, T. Ziegler (Eds.), Chemical Applications of Density Functional Theory, vol. 629, American Chemical Society, Washington, DC, 1996, p. 20.
[49] O.V. Gritsenko, R. van Leeuwen, E.J. Baerends, J. Chem. Phys. 101 (1994) 8955.
[50] P. Süle, O.V. Gritsenko, A. Nagy, E.J. Baerends, J. Chem. Phys. 103 (1995) 10085.
[51] E.J. Baerends, O.V. Gritsenko, J. Phys. Chem. A 101 (1997) 5383.
[52] M. Elian, R. Hoffmann, Inorg. Chem. 14 (1975) 1058.
[53] A. Rosa, A.W. Ehlers, E.J. Baerends, J.G. Snijders, G. te Velde, J. Phys. Chem. 100 (1996) 5690.
[54] M.S. Wrighton, D.L. Morse, H.B. Gray, D.K. Otteson, J. Am. Chem. Soc. 98 (1976) 1111.
[55] A. Berry, T.L. Brown, Inorg. Chem. 11 (1972) 1165.
[56] K. Pierloot, P. Hoet, L.G. Vanquickenborne, J. Chem. Soc. Dalton Trans. (1991) 2363.
[57] T. Matsubara, C. Daniel, A. Veillard, Organometallics 13 (1994) 4905.
[58] C. Daniel, J. Am. Chem. Soc. 114 (1992) 1625.
[59] K. Finger, C. Daniel, J. Am. Chem. Soc. 117 (1995) 12322.
[60] K. Finger, C. Daniel, P. Saalfrank, B. Schmidt, J. Phys. Chem. 100 (1996) 3368.
[61] G.J. Stor, S.L. Morrison, D.J. Stufkens, A. Oskam, Organometallics 13 (1994) 2641.
[62] A. Rosa, G. Ricciardi, E.J. Baerends, D.J. Stufkens, J. Phys. Chem. 100 (1996) 15346.
[63] A. Waldman, S. Ruhman, S. Shaik, G.N. Sastry, Chem. Phys. Lett. 230 (1994) 110.
[64] S.K. Kim, S. Pedersen, A.H. Zewail, Chem. Phys. Lett 233 (1995) 500.